INTERNATIONAL JOURNAL FOR NUMERICAL METHODS IN FLUIDS, VOL. 16, 793–811 (1993)

# THE ANALYSIS OF UNSTEADY INCOMPRESSIBLE FLOWS BY A THREE-STEP FINITE ELEMENT METHOD

CHUN BO JIANG AND MUTSUTO KAWAHARA

*Department of Civil Engineering, Chuo University, Kasuga 1-13-27, Bunkyo-ku, Tokyo 112, Japan*

SUMMARY

This paper describes a three-step finite element method and its applications to unsteady incompressible fluid flows. Stability analysis of the one-dimensional pure convection equation shows that this method has third-order accuracy and an extended numerical stability domain in comparison with the Lax–Wendroff finite element method. The method is cost-effective for incompressible flows because it permits less frequent updates of the pressure field with good accuracy. In contrast with the Taylor–Galerkin method, the present method does not contain any new higher-order derivatives, which makes it suitable for solving non-linear multidimensional problems and flows with complicated boundary conditions. The three-step finite element method has been used to simulate unsteady incompressible flows. The numerical results obtained are in good agreement with those in the literature.

KEY WORDS Three-step method Convection-dominated flows Unsteady incompressible flows Density flows

## 1. INTRODUCTION

The finite element method appears to be very convenient and most promising for obtaining spatial approximations to problems in complex geometries. However, for convection-dominated problems it has been found that combining low-order time-stepping methods with conventional Galerkin spatial discretization often fails to produce stable numerical results, because the central treatment of the first-order spatial derivatives in Galerkin formulations is not able to cope with the dominant role played by the characteristic in hyperbolic problems. In order to overcome this difficulty, upwind finite element methods have been proposed, among which the SUPG (streamline upwind/Petrov–Galerkin) formulations[1–6] are believed to be more accurate than other upwind schemes.

Another accurate method for the finite element solution of hyperbolic problems is the Taylor–Galerkin method.[7–10] For the advection equation the starting point is the substitution of space derivatives for the time derivatives in a Taylor expansion, as used in the derivation of the Lax–Wendroff method,[11] the only modification being that the procedure is carried out to third order. When combined with conventional Galerkin spatial discretization, the resulting scheme possesses the desired properties of extended stability and improved phase accuracy. Moreover, in contrast with the SUPG method, it is not necessary to modify the free parameter in the Taylor–Galerkin method.

It is notable that most applications of Taylor–Galerkin methods are second-order schemes,[12–14] which are accurate enough for many practical flows. However, second-order schemes can be only used for small values of the time step,[9] i.e. the Courant number must be less

0271–2091/93/090793–19$14.50

*Received July 1992*
*Revised November 1992*

than $1/\sqrt{3}$. The cost of using small time steps is especially burdensome for the Navier–Stokes equations, where a pressure update is required at each time step. To ease this problem, a subcycling technique was proposed by Gresho *et al.*[15] which permits less frequent updates of the pressure field with little loss of accuracy. The third-order Taylor–Galerkin scheme has an extended stability domain which is cost-efficient for incompressible flows. However, its applications are mainly to hyperbolic problems and some convection–diffusion equations,[7-9] because too many terms are introduced in the third-order time derivative term, especially for non-linear multidimensional equations, and treatments of the boundary integrations arising from high-order time derivative terms are too complicated.

A three-step finite element method based on a Taylor series expansion in time is proposed in the present study. It is not necessary to calculate any new higher-order spatial derivatives here. This makes it convenient to simulate non-linear multidimensional flows. The ideas are almost the same as those of the two-step finite element method,[16-18] but the present scheme retains the good accuracy and uniform CFL property of the Taylor–Galerkin method.[7-10] The method is cost-effective for incompressible flows since it allows less frequent updates of the pressure field with good accuracy.

Stability analysis of the one-dimensional pure convection equation is performed. The results show that the present method has third-order accuracy and an extended stability domain compared with the Lax–Wendroff finite element method. The present three-step finite element method is applied to solve incompressible laminar flows. The same order of interpolation is used for the velocity and pressure.

Before introducing the three-step finite element method, it is necessary to have a brief statement of the two-step Lax–Wendroff finite element method.

## 2. TWO-STEP LAX–WENDROFF FINITE ELEMENT METHOD

Let us consider the convection–diffusion equation

$$\frac{\partial f}{\partial t}+u_j f_{,j}=(kf_{,j})_{,j}+S_f, \tag{1}$$

where $f$ is the concentration, $u_i$ is the velocity, $k$ is the diffusion coefficient and $S_f$ is the source term. Performing a Taylor series expansion in time, we have

$$f(t+\Delta t)=f(t)+\Delta t\frac{\partial f(t)}{\partial t}+\frac{\Delta t^2}{2}\frac{\partial^2 f(t)}{\partial t^2}+\frac{\Delta t^3}{6}\frac{\partial^3 f(t)}{\partial t^3}+O(\Delta t^4). \tag{2}$$

By approximating equation (2) to second-order accuracy, the formulations of the two-step method can be derived as

$$\begin{aligned} f\left(t+\frac{\Delta t}{2}\right)&=f(t)+\frac{\Delta t}{2}\frac{\partial f(t)}{\partial t},\\ f(t+\Delta t)&=f(t)+\Delta t\frac{\partial f(t+\Delta t/2)}{\partial t}. \end{aligned} \tag{3}$$

Spatial discretization of equations (3) can be performed using the standard Galerkin finite element method. When the resulting finite element formulations are solved using the consistent mass matrix, the well-known two-step Lax–Wendroff finite element formulation is derived. This method is more accurate and stable for convection-dominated flows,[16,17] but the uniform CFL condition cannot be achieved. The stwo-step Lax-Wendroff finite element method has been

applied to calculate incompressible flow problems.[16-18] For high-Reynolds-number flows the time step $\Delta t$ should be less than $h/(|u|+|v|)$ because of the stability condition.[16]

## 3. THREE-STEP FINITE ELEMENT METHOD

By approximating equation (2) up to third-order accuracy, the formulations of the three-step method can be written as

$$f\left(t+\frac{\Delta t}{3}\right)=f(t)+\frac{\Delta t}{3}\frac{\partial f(t)}{\partial t},$$
$$f\left(t+\frac{\Delta t}{2}\right)=f(t)+\frac{\Delta t}{2}\frac{\partial f(t+\Delta t/3)}{\partial t}, \tag{4}$$
$$f(t+\Delta t)=f(t)+\Delta t\frac{\partial f(t+\Delta t/2)}{\partial t}.$$

When equations (4) are discretized using the standard Galerkin finite element method and the resulting finite element equations of the consistent mass matrix forms are solved by Jacobian iteration, the three-step finite element method is obtained. This is a new finite element method, it retains the advantages of the Taylor–Galerkin method such as third-order accuracy and the uniform CFL condition. The method is cost-efficient for incompressible flows compared with the second-order Lax–Wendroff finite element method because it permits less frequent updates of the pressure field with good accuracy. In contrast with the Taylor–Galerkin method, the three-step finite element method does not contain any new higher-order spatial derivatives and can thus be applied to solve non-linear multidimensional flows with ease.

## 4. STABILITY ANALYSIS

Spatial discretization of equations (3) and (4) can be carried out by the standard Galerkin method. In the one-dimensional pure convection case with constant velocity and using a piecewise linear finite element $h$ on a uniform mesh, the discrete formulation of equations (3) can be obtained as

$$f_i^{n+1/2}+\frac{(f_{i+1}-2f_i+f_{i-1})^{n+1/2}}{6}=f_i^n+\frac{(f_{i+1}-2f_i+f_{i-1})^n}{6}-C_r\frac{f_{i+1}^n-f_{i-1}^n}{4},$$
$$f_i^{n+1}+\frac{(f_{i+1}-2f_i+f_{i-1})^{n+1}}{6}=f_i^n+\frac{(f_{i+1}-2f_i+f_{i-1})^n}{6}-C_r\frac{f_{i+1}^{n+1/2}-f_{i-1}^{n+1/2}}{2}, \tag{5}$$

where $C_r=u\Delta t/h$ is the Courant number and $f_i$ is the concentration value at point $i$. In order to perform a Fourier analysis, let $f_i^n=V^n e^{ijhp}=V^n e^{ij\xi}$, where $j=\sqrt{(-1)}$, $p$ is the wave number and $\xi=hp$, so that the amplification factor $g(\xi, C_r)$ is defined by $V^{n+1}=g(\xi, C_r)V^n$. For equations (5) the formulation

$$g(\xi, C_r)=1-\frac{1}{2}\left(\frac{C_r\sin\xi}{1-\frac{2}{3}\sin^2(\xi/2)}\right)^2-j\frac{C_r\sin\xi}{1-\frac{2}{3}\sin^2(\xi/2)} \tag{6}$$

can be derived, which in the asymptotic limit $\xi\to 0$ reduces to

$$g(\xi, C_r)=1-jC_r\xi-\tfrac{1}{2}C_r^2\xi^2+\ldots. \tag{7}$$

This shows that the two-step Lax–Wendroff finite element method is globally second-order-accurate. The analytical solution of the pure convection equation can be assumed as

$f(x,t)=X(x)T(t)=Ae^{jp(x-ut)}$, where $A$ is a constant; thus the analytical amplification factor $g_a(\xi, C_r)$ can be obtained as $g_a(\xi, C_r)=f(x_i, t^{n+1})/f(x_i, t^n)=e^{-jpu\Delta t}=e^{-jC_r\xi}$. By rewriting $g(\xi, C_r)=|g|e^{-j\psi(\xi, C_r)}$, the nature of the phase errors and dissipation errors in the schemes can be examined. The amplification error $\rho$ is defined as $\rho(\xi, C_r)=|g|/|g_a|=|g|$ and the phase error $\phi$ is defined as $\phi(\xi, C_r)=\arg(g)/\arg(g_a)=\psi/C_r\xi$. The condition of numerical stability $\rho\leqslant 1$ leads to $C_r\leqslant 1/\sqrt{3}$,[9] to be compared with the condition $C_r\leqslant 1$ of the Lax–Wendroff finite difference method. The reduction of the stability domain is due to the presence in the finite element equations of the consistent mass matrix, which endows the scheme with fourth-order spatial accuracy.[9,10] Following the same procedure as for the two-step Lax–Wendroff finite element method, the discretized formulations of the three-step finite element method expressed by equations (4) are obtained as

$$
\begin{aligned}
f_i^{n+1/3}+\frac{(f_{i+1}-2f_i+f_{i-1})^{n+1/3}}{6}&=f_i^n+\frac{(f_{i+1}-2f_i+f_{i-1})^n}{6}-C_r\frac{f_{i+1}^n-f_{i-1}^n}{6},\\
f_i^{n+1/2}+\frac{(f_{i+1}-2f_i+f_{i-1})^{n+1/2}}{6}&=f_i^n+\frac{(f_{i+1}-2f_i+f_{i-1})^n}{6}-C_r\frac{f_{i+1}^{n+1/3}-f_{i-1}^{n+1/3}}{6},\\
f_i^{n+1}+\frac{(f_{i+1}-2f_i+f_{i-1})^{n+1}}{6}&=f_i^n+\frac{(f_{i+1}-2f_i+f_{i-1})^n}{6}-C_r\frac{f_{i+1}^{n+1/2}-f_{i-1}^{n+1/2}}{2},
\end{aligned}
\tag{8}
$$

again let $f_i^n=V^ne^{ijhp}=V^ne^{ij\xi}$, so that the amplification factor $g(\xi, C_r)$ of equations (8) can be derived as

$$
g(\xi, C_r)=1-\frac{1}{2}\left(\frac{C_r\sin\xi}{1-\frac{2}{3}\sin^2(\xi/2)}\right)^2-j\left[\frac{C_r\sin\xi}{1-\frac{2}{3}\sin^2(\xi/2)}-\frac{1}{6}\left(\frac{C_r\sin\xi}{1-\frac{2}{3}\sin^2(\xi/2)}\right)^3\right],
\tag{9}
$$

which in the asymptotic limit $\xi\to 0$ reduces to

$$
g(\xi, C_r)=1-jC_r\xi-\tfrac{1}{2}C_r^2\xi^2+\tfrac{1}{6}jC_r^3\xi^3+\ldots.
\tag{10}
$$

By comparison with $e^{-jC_r\xi}$ for the differential equation, it follows that the three-step finite element method is third-order-accurate. In Figure 1 the amplification error $\rho$ and the phase error $\phi$ are compared for the two-step Lax–Wendroff finite element method and the three-step finite element method. These figures show that the three-step finite element method is stable for $0\leqslant C_r\leqslant 1$, but that the two-step Lax–Wendroff finite element method is unstable for $C_r\geqslant 0{\cdot}5$. Thus the third-order correction extends the stability domain with respect to the second-order Lax–Wendroff finite element method and ensures the unit CFL condition. The phase shift of the Taylor–Galerkin method is zero for $C_r=0{\cdot}5$ and $1{\cdot}0$. However, the phase shift of the three-step finite element method is negative at intermediate and short wavelengths, which is almost the same as that of the two-step Lax–Wendroff finite element method. In practical simulations it is very difficult to keep the Courant number as a constant; thus the relatively poor phase error of the three-step method for $C_r=0{\cdot}5$ and $1{\cdot}0$ is not serious.

## 5. PURE CONVECTION FLOW

In order to display the accuracy of the three-step finite element method, the pure convection movement of a cosine hill in a rotating flow field is presented. The pure convection equation is expressed as

$$
\frac{\partial f}{\partial t}=-u_jf_{,j},
\tag{11}
$$

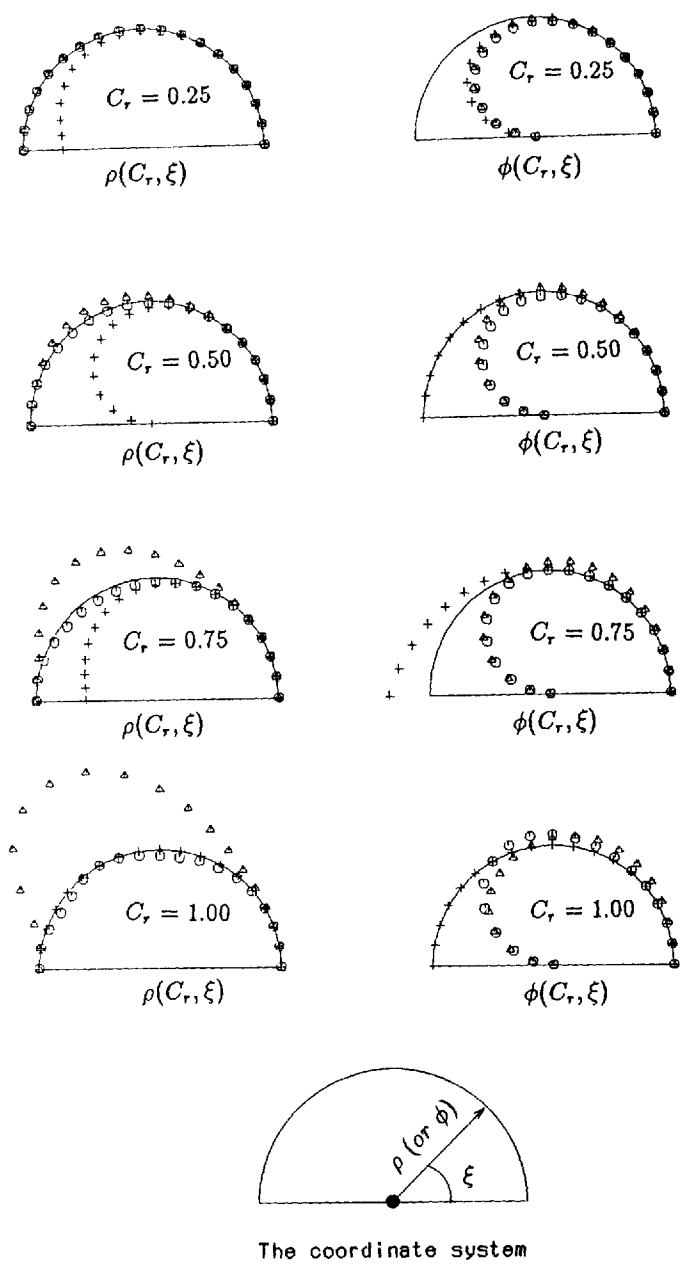


Figure 1. Amplification error $\rho$ (left) and phase error $\phi$ (right): ○; three-step FE method; △, two-step FE method; +, Taylor–Galerkin method

where the velocity $u_j$ is defined as

$$u_1 = -x_2, \qquad u_2 = x_1. \tag{12}$$

A uniform grid of $30 \times 30$ is used and the initial (also exact) distribution of the hill is shown in Figure 2(a). On the basis of equations (8), the three-step finite element formulations can be

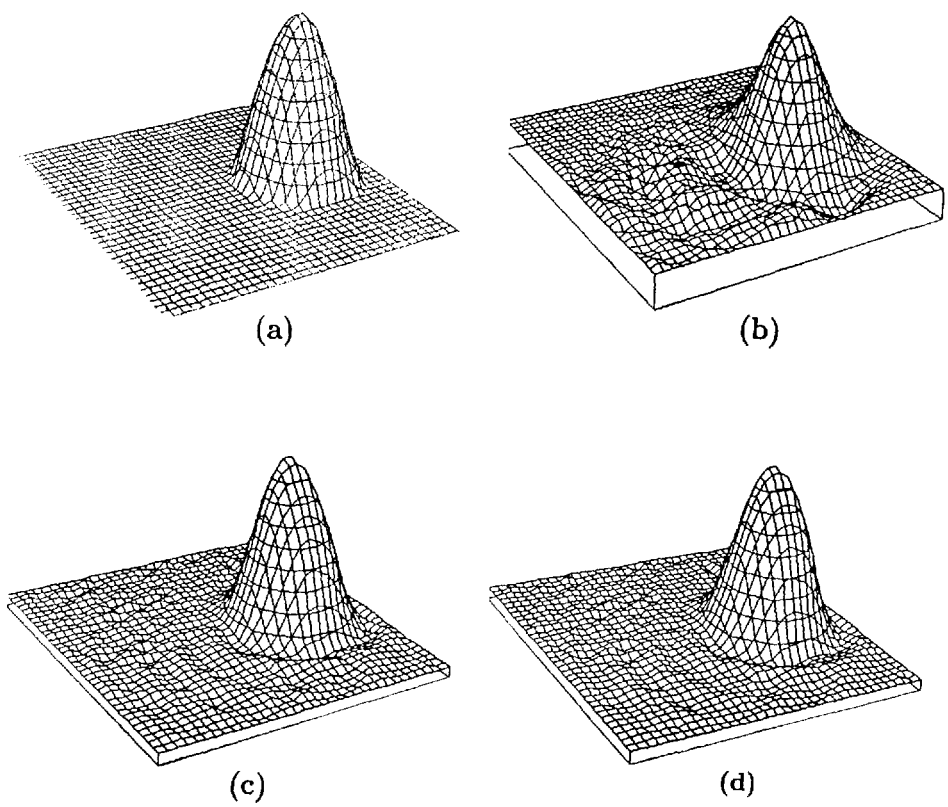


Figure 2. Shapes of the hill after one rotation: (a) initial (or exact) distribution of the hill; (b) by two-step FE method (lumping), $\Delta t = 0{\cdot}0157$; (c) by two-step FE method, $\Delta t = 0{\cdot}0157$; (d) by three-step FE method, $\Delta t = 0{\cdot}0314$

expressed as

$$\begin{aligned} f^{n+1/3} &= f^n - \frac{\Delta t}{3} u_j f^n_{,j}, \\ f^{n+1/2} &= f^n - \frac{\Delta t}{2} u_j f^{n+1/3}_{,j}, \\ f^{n+1} &= f^n - \Delta t u_j f^{n+1/2}_{,j}. \end{aligned} \tag{13}$$

Spatial discretization of equations (13) is performed using the standard Galerkin method. The resulting finite element equations are obtained as

$$\begin{aligned} M_{\alpha\beta}(f^{n+1/3}_\beta - f^n_\beta) &= -\frac{\Delta t}{3} N_{\alpha\beta} f^n_\beta, \\ M_{\alpha\beta}(f^{n+1/2}_\beta - f^n_\beta) &= -\frac{\Delta t}{2} N_{\alpha\beta} f^{n+1/3}_\beta, \\ M_{\alpha\beta}(f^{n+1}_\beta - f^n_\beta) &= -\Delta t N_{\alpha\beta} f^{n+1/2}_\beta, \end{aligned} \tag{14}$$

where the matrices $M_{\alpha\beta}$ and $N_{\alpha\beta}$ are defined as

$$M_{\alpha\beta}=\int_{V^e}\Phi_\alpha\Phi_\beta\,\mathrm{d}V, \qquad N_{\alpha\beta}=\int_{V^e}\Phi_\alpha\Phi_\gamma\Phi_{\beta,j}u_{j\gamma}\,\mathrm{d}V. \tag{15}$$

Here $V^e$ is the element domain and $\Phi_\alpha$ is a linear interpolation function defined as

$$\Phi_\alpha=a_\alpha+b_\alpha x_1+c_\alpha x_2, \tag{16}$$

where $a_\alpha$, $b_\alpha$ and $c_\alpha$ are the parameters of the element geometry. For the two-step finite element method, when the lumping mass matrix is used instead of the consistent mass matrix, the resulting scheme is the same as the Lax–Wendroff finite difference scheme. Figure 2(b) shows the results obtained by the lumping finite element method. The time step $\Delta t$ is 0·0157 s. The oscillations are about 25% of the height of the hill for one rotation. Because the oscillations grow so fast with time, no results can be achieved after two rotations. The presence of the consistent mass matrix in the finite element method makes it possible to improve the accuracy significantly. This has been verified by numerical experiments.[12] The finite element equations are solved by Jacobian interation;[16] three iterations are carried out in the calculations. The result obtained by the two-step finite element method is shown in Figure 2(c); a small value of $\Delta t$ (0·0157 s) is used in order to achieve a stable solution. After one rotation the oscillations at the foot of the hill are about 7% of the height of the hill. The CPU time for one rotation is 15·2 s on the FACOM VP-30 computer. For the three-step method the relatively large time step $\Delta t=0{\cdot}0314$ s is used. The calculated results of one rotation are shown in Figure 2(d). This figure shows that the three-step method is stable for a larger time step, but there is no improvement in the accuracy. The shape of the hill is almost the same as that obtained by the two-step method even if the larger time step is used. It costs 11·5 s of CPU time on the same computer for one rotation, which is 75% of that for the two-step method.

## 6. INCOMPRESSIBLE FLOWS

For incompressible flows, as we know, the pressure is usually determined by a derived Poisson equation, which is the most time-consuming procedure in one time step. Since the present three-step method allows the use of a larger time step than that of second-order finite element schemes,[12–14,16,17] this results in a reduction in the total CPU time. The flows are governed by the Navier–Stokes equations

$$\frac{\partial u_i}{\partial t}+u_ju_{i,j}=-\frac{p_{,i}}{\rho}+\nu(u_{i,j}+u_{j,i})_{,j}+f_i \quad \text{in } V, \tag{17}$$

$$u_{i,i}=0 \quad \text{in } V, \tag{18}$$

where $V$ is the computational domain, $u_i$ is the velocity component in the $x_i$-co-ordinate direction, $f_i$ is the external force, $t$ is time, $p$ is the pressure, $\rho$ is the fluid density and $\nu$ is the kinematic viscosity of the fluid. The boundary conditions are

$$u_i=\hat{u}_i \quad \text{on } S_1,$$

$$\sigma_{ij}=-\frac{p\delta_{ij}}{\rho}+\nu(u_{i,j}+u_{j,i})=\hat{\sigma}_{ij} \quad \text{on } S_2, \tag{19}$$

where $\sigma_{ij}$ is the stress, $S_1$ and $S_2$ are two disjoint non-overlapping subsets of the boundary $S$ and the circumflex indicates the prescribed value on the boundary. By applying the three-step finite

element method, the following discretized equations can be obtained:

$$\begin{aligned}
\frac{u_i^{n+1/3}-u_i^n}{\Delta t/3} &= -u_j^n u_{i,j}^n - \frac{p_{,i}^n}{\rho} + \nu(u_{i,j}^n + u_{j,i}^n)_{,j} + f_i^n,\\
\frac{u_i^{n+1/2}-u_i^n}{\Delta t/2} &= -u_j^{n+1/3} u_{i,j}^{n+1/3} - \frac{p_{,i}^n}{\rho} + \nu(u_{i,j}^{n+1/3} + u_{j,i}^{n+1/3})_{,j} + f_i^{n+1/3},\\
\frac{u_i^{n+1}-u_i^n}{\Delta t} &= -u_j^{n+1/2} u_{i,j}^{n+1/2} - \frac{p_{,i}^{n+1}}{\rho} + \nu(u_{i,j}^{n+1/2} + u_{j,i}^{n+1/2})_{,j} + f_i^{n+1/2}.
\end{aligned} \tag{20}$$

Spatial discretization of equations (20) can be performed using the standard Galerkin method. The resulting finite element equations can be expressed as

$$\begin{aligned}
M_{\alpha\beta}\frac{u_{i\beta}^{n+1/3}-u_{i\beta}^n}{\Delta t/3} &= -N_{\alpha\beta}^n u_{i\beta}^n + \frac{L_{i\alpha\beta}p_\beta^n}{\rho} - \nu S_{i\alpha}^n + M_{\alpha\beta}f_{i\beta}^n\\
&\quad -\frac{1}{\rho}\int_S \Phi_\alpha p^n \cdot n_i \,\mathrm{d}S + \int_S \Phi_\alpha \nu(u_{i,j}^n + u_{j,i}^n)\cdot n_j \,\mathrm{d}S,\\
M_{\alpha\beta}\frac{u_{i\beta}^{n+1/2}-u_{i\beta}^n}{\Delta t/2} &= -N_{\alpha\beta}^{n+1/3} u_{i\beta}^{n+1/3} + \frac{L_{i\alpha\beta}p_\beta^n}{\rho} - \nu S_{i\alpha}^{n+1/3} + M_{\alpha\beta}f_{i\beta}^{n+1/3}\\
&\quad -\frac{1}{\rho}\int_S \Phi_\alpha p^n \cdot n_i \,\mathrm{d}S + \int_S \Phi_\alpha \nu(u_{i,j}^{n+1/3} + u_{j,i}^{n+1/3})\cdot n_j \,\mathrm{d}S,\\
M_{\alpha\beta}\frac{u_{i\beta}^{n+1}-u_{i\beta}^n}{\Delta t} &= -N_{\alpha\beta}^{n+1/2} u_{i\beta}^{n+1/2} + \frac{L_{i\alpha\beta}p_\beta^{n+1}}{\rho} - \nu S_{i\alpha}^{n+1/2} + M_{\alpha\beta}f_{i\beta}^{n+1/2}\\
&\quad -\frac{1}{\rho}\int_S \Phi_\alpha p^{n+1} \cdot n_i \,\mathrm{d}S + \int_S \Phi_\alpha \nu(u_{i,j}^{n+1/2} + u_{j,i}^{n+1/2})\cdot n_j \,\mathrm{d}S,
\end{aligned} \tag{21}$$

where $n_i$ is the component of the unit vector normal to the boundary. The elemental matrix $M_{\alpha\beta}$ is expressed by the first of equations (15) and $L_{i\alpha\beta}$, $N_{\alpha\beta}^n$ and $S_{i\alpha}^n$ are defined as

$$\begin{aligned}
L_{i\alpha\beta} &= \int_{V^e} \Phi_{\alpha,i}\Phi_\beta \,\mathrm{d}V,\\
N_{\alpha\beta}^n &= \int_{V^e} \Phi_\alpha \Phi_\gamma \Phi_{\beta,j} u_{j\gamma}^n \,\mathrm{d}V,\\
S_{i\alpha}^n &= \int_{V^e} \Phi_{\alpha,j}(\Phi_{\beta,j}u_{i\beta}^n + \Phi_{\beta,i}u_{j\beta}^n)\,\mathrm{d}V.
\end{aligned} \tag{22}$$

Before calculating the velocity $u_i^{n+1}$ from the last formulation of equations (20), the pressure $p^{n+1}$ has to be solved. By taking the divergence on both sides of the last formulation of equation (20) and introducing the incompressibility constraint $u_{i,i}^{n+1}=0$, the following Poisson equation of pressure is derived:

$$\frac{p_{,ii}^{n+1}}{\rho} = \frac{u_{i,i}^n}{\Delta t} - (u_j^{n+1/2}u_{i,j}^{n+1/2})_{,i} + \nu(u_{i,j}^{n+1/2} + u_{j,i}^{n+1/2})_{,ij} + f_{i,i}^{n+1/2}. \tag{23}$$

By using the Galerkin finite element method, the weak formulation of equation (23) is obtained as

$$\int_V \frac{p^*_{,i}p^{n+1}_{,i}}{\rho}\,dV = -\frac{1}{\Delta t}\int_V p^* u^n_{i,i}\,dV - \int_V p^*_{,i}u^{n+1/2}_j u^{n+1/2}_{i,j}\,dV + \int_V \nu p^*_{,i}(u^{n+1/2}_{i,j}+u^{n+1/2}_{j,i})_{,j}\,dV$$
$$+\int_V p^*_{,i}f^{n+1/2}_i\,dV + \int_S p^*\left(u^{n+1/2}_j u^{n+1/2}_{i,j}\right.$$
$$\left.-\nu(u^{n+1/2}_{i,j}+u^{n+1/2}_{j,i})_{,j} - f^{n+1/2}_i + \frac{p^{n+1}_{,i}}{\rho}\right)\cdot n_i\,dS, \tag{24}$$

where $p^*$ is the weighting function of pressure. Since the pressure is solved from a Poisson equation, it is possible to use the same order of interpolation for the velocity and pressure instead of mixed order interpolation.[19] By using the last formulation of equations (20), the normal gradient of pressure can be expressed as

$$p^{n+1}_{,i}\rho^{-1}\cdot n_i = -\frac{u^{n+1}_i - u^n_i}{\Delta t}\cdot n_i - u^{n+1/2}_j u^{n+1/2}_{i,j}\cdot n_i + \nu(u^{n+1/2}_{i,j}+u^{n+1/2}_{j,i})_{,j}\cdot n_i + f^{n+1/2}_i\cdot n_i. \tag{25}$$

Substitution of equation (25) into (24) results in

$$\int_V p^*_{,i}p^{n+1}_{,i}\rho^{-1}\,dV = -\frac{1}{\Delta t}\int_V p^* u^n_{i,i}\,dV - \int_V p^*_{,i}u^{n+1/2}_j u^{n+1/2}_{i,j}\,dV$$
$$+\int_V p^*_{,i}f^{n+1/2}_i\,dV - \int_S p^*\frac{u^{n+1}_i - u^n_i}{\Delta t}\cdot n_i\,dS \tag{26}$$

For most cases the boundary integration part of (26) is non-zero only on the outlet boundary. Detailed discussion of the pressure boundary conditions can be found in References 19 and 20. The final finite element formulation of (26) is

$$\frac{G_{\alpha\beta}p^{n+1}_\beta}{\rho} = -\frac{1}{\Delta t}H_{i\alpha\beta}u^n_{i\beta} - K_{j\alpha\beta}u^{n+1/2}_{j\beta} - \Omega_\alpha, \tag{27}$$

where the elemental matrices are

$$H_{i\alpha\beta} = \int_{V^e}\Phi_\alpha\Phi_{\beta,i}\,dV, \qquad K_{j\alpha\beta} = \int_{V^e}\Phi_{\alpha,i}\Phi_\beta\Phi_{\gamma,j}u_{i\gamma}\,dV,$$
$$G_{\alpha\beta} = \int_{V^e}\Phi_{\alpha,i}\Phi_{\beta,i}\,dV, \qquad \Omega_\alpha = \int_{S^e}\Phi_\alpha\frac{u^{n+1}_i - u^n_i}{\Delta t}\cdot n_i\,dS. \tag{28}$$

### 6.1. *Cavity flows*

In order to confirm the accuracy and the computational efficiency of the three-step method, cavity flows with Reynolds numbers $Re = 400$ and 1000 are calculated. For $Re = 400$ a uniform grid of $21 \times 21$ and a time step $\Delta t = 0{\cdot}05$ are used. The corresponding maximum Courant number is 1·3. The velocity vector, pressure contour lines, streamlines and steady state velocity profiles are shown in Figures 3(a)–3(d) respectively. The minimum streamfunction value ($\Psi_{\min}$), the location of the vortex centre ($x_c$, $y_c$), the maximum and minimum vertical velocity components ($V_{\max}$ and $V_{\min}$) along the horizontal centreline ($x$, 0·5) and the minimum horizontal velocity component ($U_{\min}$) along the vertical centreline (0·5, $y$) are compared with the literature values[16,21–23] in Table I. For $Re = 1000$ a refined uniform $41 \times 41$ mesh and a time step $\Delta t = 0{\cdot}025$ are used. The

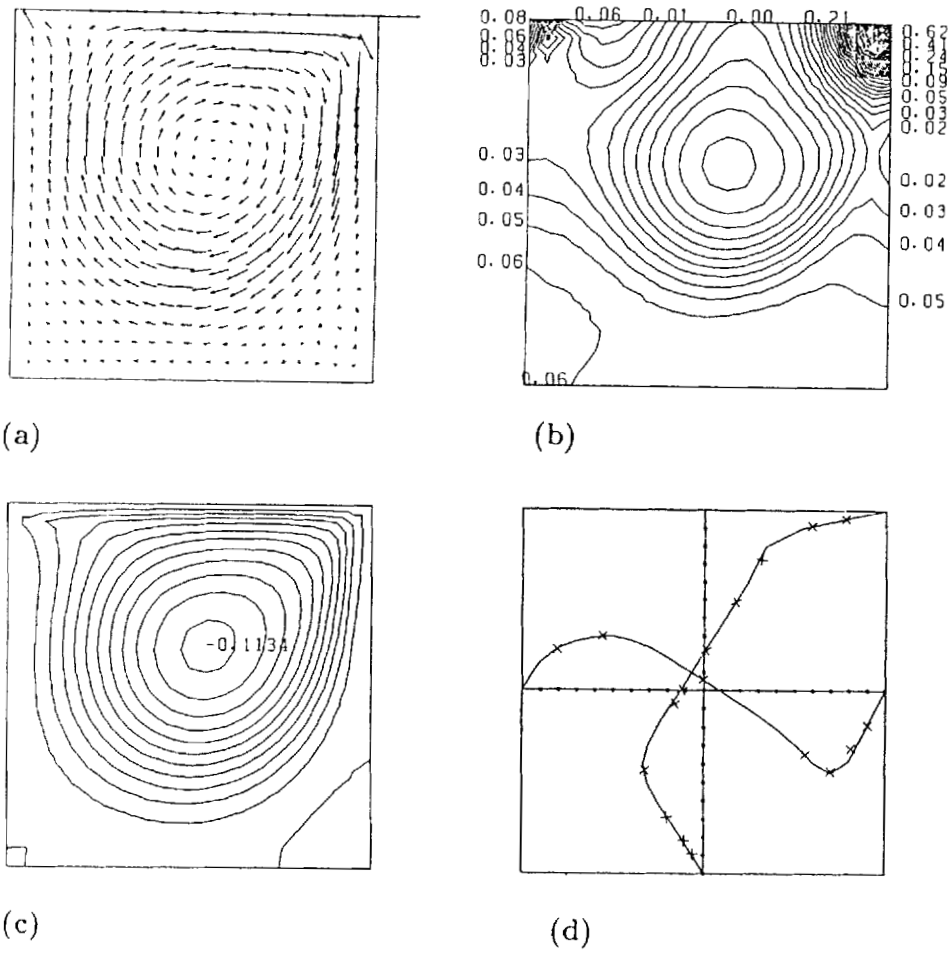


Figure 3. Steady solutions of cavity flow with $Re=400$: (a) velocity vector; (b) pressure contour lines; (c) streamlines; (d) velocity profiles ( $\times$, Reference 23)

Table I. Main properties of cavity flow with $Re=400$

| Scheme | Grid | $\Psi_{min}$ | $(x_c, y_c)$ | $U_{min}$ | $V_{min}$ | $V_{max}$ |
|---|---|---|---|---|---|---|
| Reference 16 | $41\times41$ | $-0{\cdot}1012$ | (0·55, 0·60) | $-0{\cdot}285$ | $-0{\cdot}390$ | 0·250 |
| Reference 21 | $33\times17$ | $-0{\cdot}1136$ | (0·55, 0·60) | $-0{\cdot}335$ | $-0{\cdot}50$ | 0·275 |
| Reference 22 | $67\times67$ | $-0.112$ | (0·56, 0·62) | $-0{\cdot}300$ | $-0{\cdot}450$ | 0·293 |
| Reference 23 | $129\times129$ | $-0{\cdot}1139$ | (0·56, 0·61) | $-0{\cdot}327$ | $-0{\cdot}450$ | 0·302 |
| Present | $21\times21$ | $-0{\cdot}1134$ | (0·56, 0·62) | $-0{\cdot}310$ | $-0{\cdot}450$ | 0·294 |

calculated steady results, i.e. the velocity vector, pressure contour lines, streamlines and velocity profiles, are shown in Figures 4(a)–(4(d) respectively. The main properties of the cavity flow are compared in Table II. The present calculations are in agreement with the literature values.[23,24]

From equations (20) and (23) it can be found that only the pressure value $p^{n+1}$ is solved for one time iteration; this results in computational efficiency. The loss of third-order accuracy by not having $p^{n+1/3}$ and $p^{n+1/2}$ in the first and second formulations of (20) may introduce an intolerable

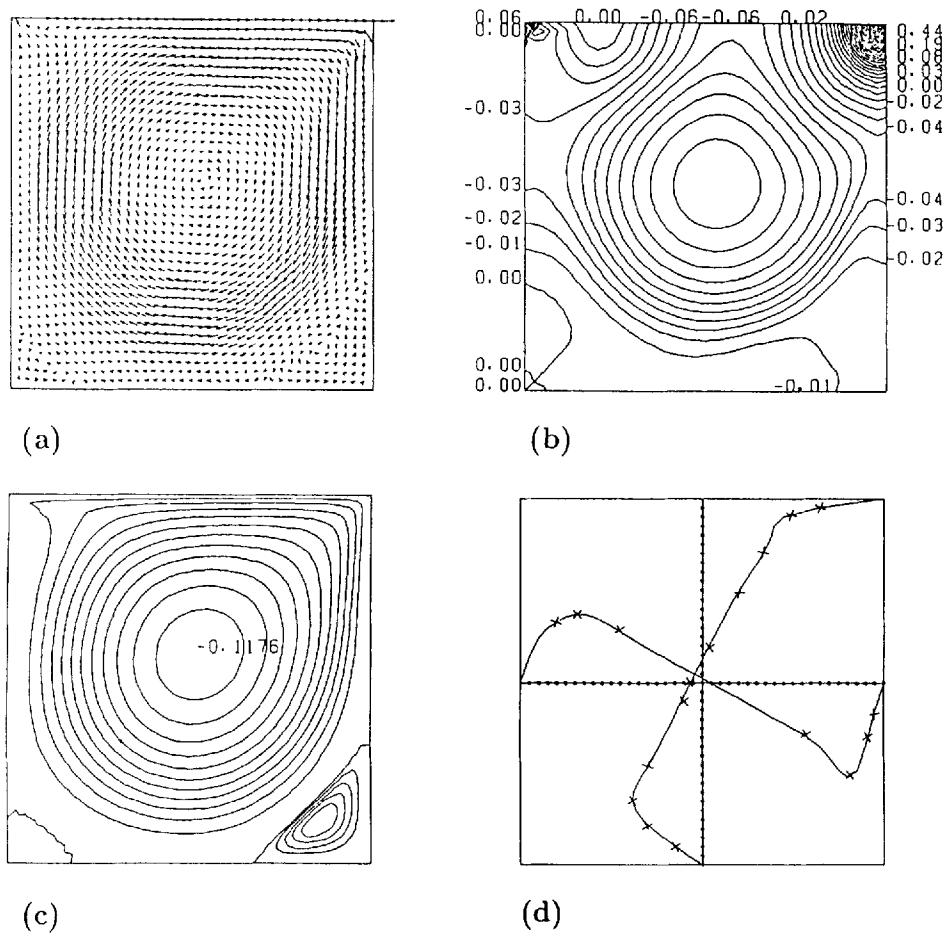


Figure 4. Steady solutions of cavity flow with $Re = 1000$: (a) velocity vector; (b) pressure contour lines; (c) streamlines; (d) velocity profiles ($\times$, Reference 23)

Table II. Main properties of cavity flow with $Re = 1000$

| Scheme | Grid | $\Psi_{min}$ | $(x_c, y_c)$ | $U_{min}$ | $V_{min}$ | $V_{max}$ |
|---|---|---|---|---|---|---|
| Reference 23 | $129 \times 129$ | $-0{\cdot}1179$ | (0·53, 0·56) | $-0{\cdot}383$ | $-0{\cdot}516$ | 0·371 |
| Reference 24 | $141 \times 141$ | $-0{\cdot}1160$ | (0·53, 0·56) | $-0{\cdot}367$ | $-0{\cdot}516$ | 0·358 |
| Present | $41 \times 41$ | $-0{\cdot}1176$ | (0·53, 0·56) | $-0{\cdot}383$ | $-0{\cdot}516$ | 0·366 |

error. In order to check the accuracy of the present three-step method, a modified three-step method can be derived as follows.

*Step 1 (modified)*

$$\frac{p^{n+1/3}_{,ii}}{\rho} = \frac{3u^n_{i,i}}{\Delta t} - (u^n_j u^n_{i,j})_{,i} + \nu(u^n_{i,j} + u^n_{j,i})_{,ij} + f^n_{i,i},$$
$$\frac{u^{n+1/3}_i - u^n_i}{\Delta t/3} = -u^n_j u^n_{i,j} - \frac{p^{n+1/3}_{,i}}{\rho} + \nu(u^n_{i,j} + u^n_{j,i})_{,j} + f^n_i. \tag{29}$$

*Step 2 (modified)*

$$\frac{p^{n+1/2}_{,ii}}{\rho}=\frac{2u^{n}_{i,i}}{\Delta t}-(u^{n+1/3}_{j}u^{n+1/3}_{i,j})_{,i}+\nu(u^{n+1/3}_{i,j}+u^{n+1/3}_{j,i})_{,ij}+f^{n+1/3}_{i,i},$$
$$\frac{u^{n+1/2}_{i}-u^{n}_{i}}{\Delta t/2}=-u^{n+1/3}_{j}u^{n+1/3}_{i,j}-\frac{p^{n+1/2}_{,i}}{\rho}+\nu(u^{n+1/3}_{i,j}+u^{n+1/3}_{j,i})_{,j}+f^{n+1/3}_{i}. \tag{30}$$

*Step 3 (modified)*

$$\frac{p^{n+1}_{,ii}}{\rho}=\frac{u^{n}_{i,i}}{\Delta t}-(u^{n+1/2}_{j}u^{n+1/2}_{i,j})_{,i}+\nu(u^{n+1/2}_{i,j}+u^{n+1/2}_{j,i})_{,ij}+f^{n+1/2}_{i,i},$$
$$\frac{u^{n+1}_{i}-u^{n}_{i}}{\Delta t}=-u^{n+1/2}_{j}u^{n+1/2}_{i,j}-\frac{p^{n+1}_{,i}}{\rho}+\nu(u^{n+1/2}_{i,j}+u^{n+1/2}_{j,i})_{,j}+f^{n+1/2}_{i}. \tag{31}$$

In the above modified three-step method the pressure values $p^{n+1/3}$, $p^{n+1/2}$ and $p^{n+1}$ are solved before solving $u_i^{n+1/3}$, $u_i^{n+1/2}$ and $u_i^{n+1}$. For the case of $Re=1000$, four points A (0·25, 0·75), B (0·75, 0·75), C (0·75, 0·25) and D (0·25, 0·25) are chosen as observation positions. For two-dimensional cavity flows the mesh division can be expressed by $m \times m$, where $m$ is the nodal division number in one direction ($x$ or $y$). The same time step $\Delta t(m)$ is used for the present three-step method and the modified three-step method, where $\Delta t(m)$ is a function of the nodal division number, while a relatively smaller time step $0{\cdot}6\Delta t(m)$ is used for the two-step method.[16] The calculations are carried until $t=37{\cdot}5$ s, at which time the steady state velocity field is obtained. The time histories of velocity and pressure are plotted in Figures 5(a) and 5(b) respectively. These figures compare the results obtained by the different methods; the speeds of convergence are almost the same. In Figure 5(a) a very small velocity difference can be found only at point C during the development stage. For the pressure history (Figure 5(b)) a difference can be seen only at point B, the peak value obtained by the modified method being about 2% larger than that of both the three-step and two-step methods. These results show that the three-step method is accurate enough without considering the values. $p^{n+1/3}$ and $p^{n+1/2}$. In the present two-dimensional simulation the non-iterative solver is used for the Poisson equation. The CPU time versus the nodal division number $m$ is plotted in Figure 6. It can be seen that the three-step method is computationally efficient as the nodal number increases. The two-step method costs more CPU time owing to its limited stability domain. The modified three-step method is most expensive because of the effort required to solve the pressure Poisson equation.

Owing to the extremely simple algorithm of the three-step method, it can be used for three-dimensional calculations without any modification. For three-dimensional flows the iterative solver is often used to solve the pressure Poisson equation, which means that much more CPU time is needed for this procedure. It is expected that the present three-step method is more efficient for three-dimensional problems.

### *6.2. Unsteady density flow*

A density flow can be described as the stable parallel gravity flow of one fluid relative to another that results from small differences in their densities. Examples include a muddy underflow in a lake or ocean, a volcanic ash flow, a moving atmospheric cold front and the mixing of fluids in many chemical engineering circumstances. The numerical example adopted here is illustrated in Figure 7. The two-dimensional calculations[25] make use of a square container. The width $B$ of the container is 48 units and the fluid depth $H$ at initial times is 16 units. At initial times

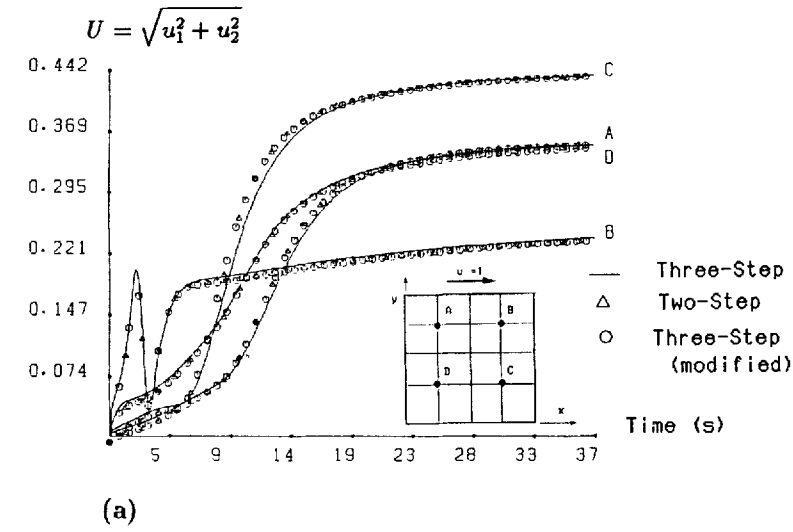


(a)

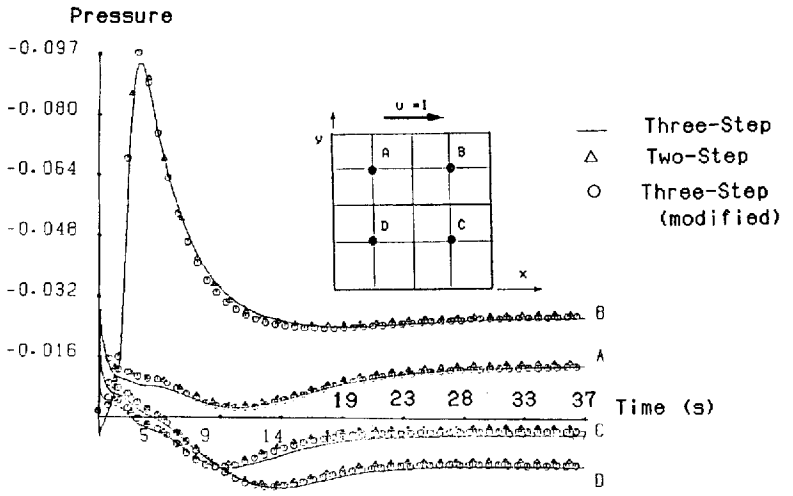


(b)

Figure 5. Time history of cavity flow with $Re = 1000$: (a) velocity versus time, (b) pressure versus time

a fluid of density $\rho_1 = 1{\cdot}0$ t m$^{-3}$ occupies the left-hand two-thirds of the container and a heavier fluid of density $\rho_2 = 1{\cdot}2$ t m$^{-3}$ occupies the right-hand one-third of the container. The gravitational acceleration $g = 9{\cdot}8$ m s$^{-2}$ is directed vertically downwards. The uniform computational grid consists of $21 \times 61$ nodal points. A time step $\Delta t = 0{\cdot}04$ is used. The CPU time for one time iteration is about 0·11 s using the FACOM VP-30 computer. The movements of the fluids are illustrated by markers. The region occupied by the heavy fluid is indicated by small circles (○), while small crosses (×) identify the lighter fluid. The movement of a marker is described by

$$x_i^{n+1} = x_i^n + \Delta t(u_i^{n+1} + u_i^n)/2. \tag{32}$$

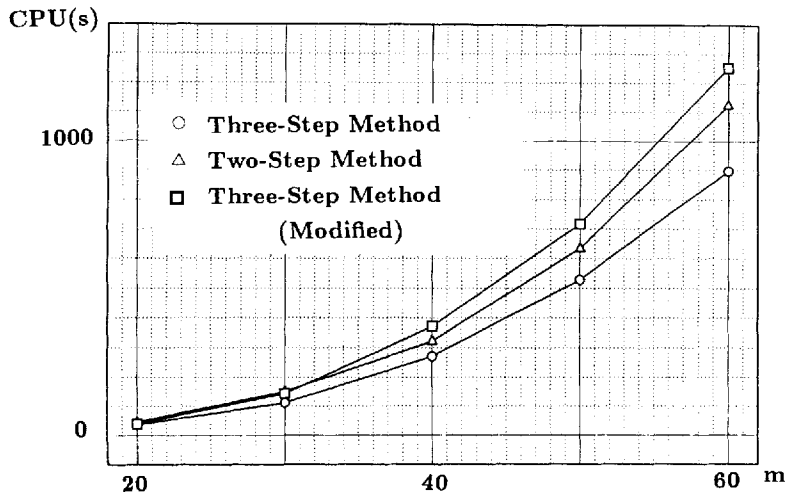


Figure 6. CPU time versus nodal division number $m$ (2D cavity flow with $m \times m$ nodal points)

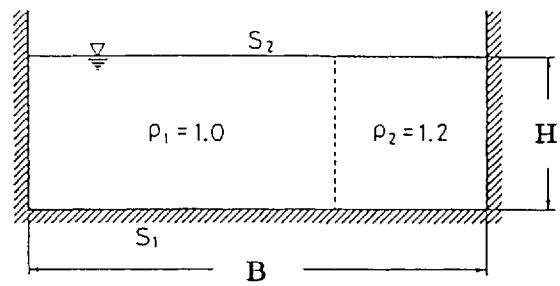


Figure 7. Schematic diagram of density flow

The computation procedure is similar to that for the one-fluid case and the density of the fluid in an element is calculated from

$$\rho = \frac{m_1 \rho_1 + m_2 \rho_2}{m_1 + m_2}, \tag{33}$$

where $m_1$ is the number of markers in an element with density $\rho_1$ and $m_2$ is the number of markers with density $\rho_2$. The buoyancy effect of variations in density is accounted for by a Boussinesq approximation to the Navier–Stokes equations (17), i.e. we replace the external force $f_i$ by

$$f_i = -\delta_{i3} g \Delta\rho, \tag{34}$$

where $\Delta\rho = (\rho - \rho_1)/\rho_0$ and $\rho_0$ is the mean density value over the whole domain. The main properties of the flow field are determined by the densimetric Froude number $R_\rho$ defined as

$$R_\rho = \frac{H\sqrt{(gH\Delta\rho/\rho_1)}}{v}. \tag{35}$$

By taking the viscosity values $v = 0{\cdot}45$, $0{\cdot}3$ and $0{\cdot}1$, the cases of densimetric Froude number $R_\rho = 200$, 300 and 900 are calculated in the present study. Since the free surface has a noticeable

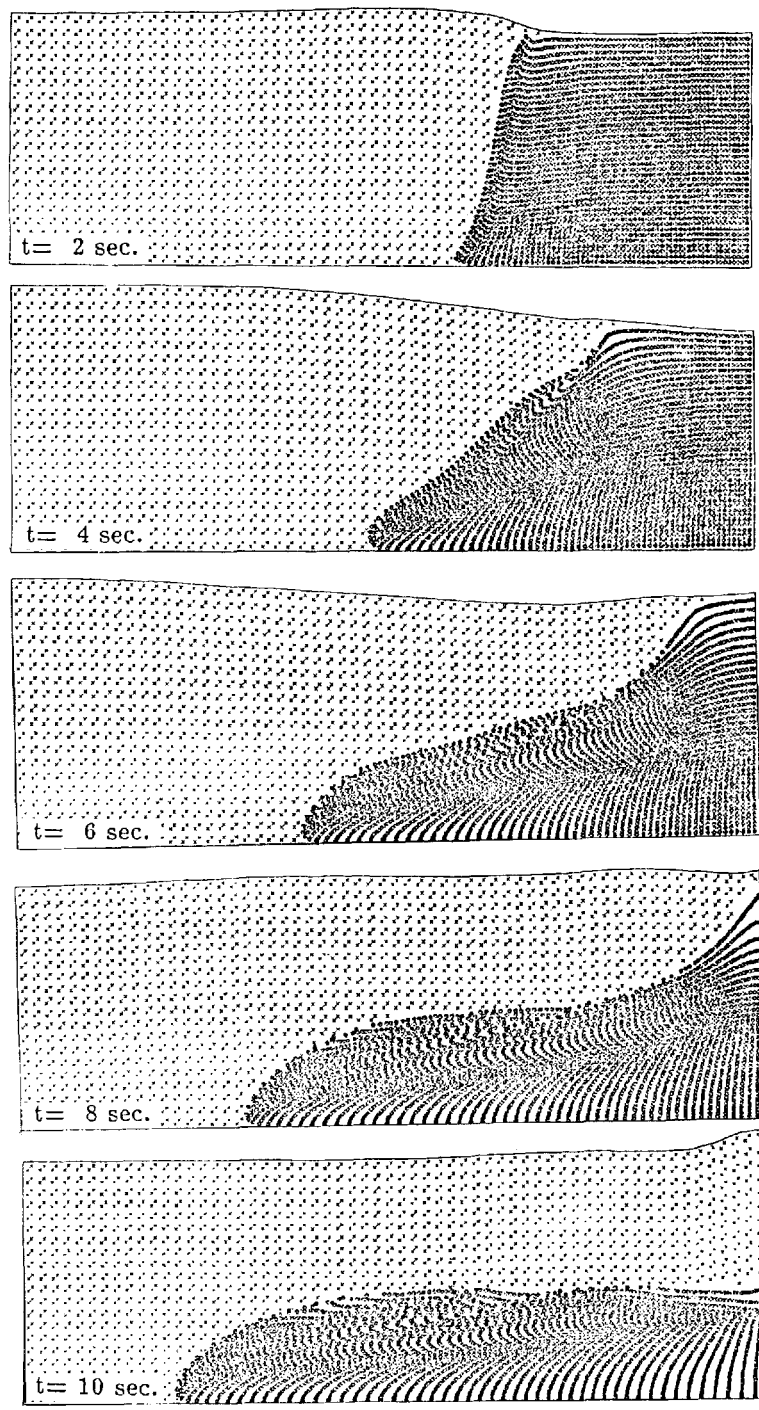


Figure 8. Density front at times $t=2$, 4, 6, 8 and 10 s ($R_\rho=200$)

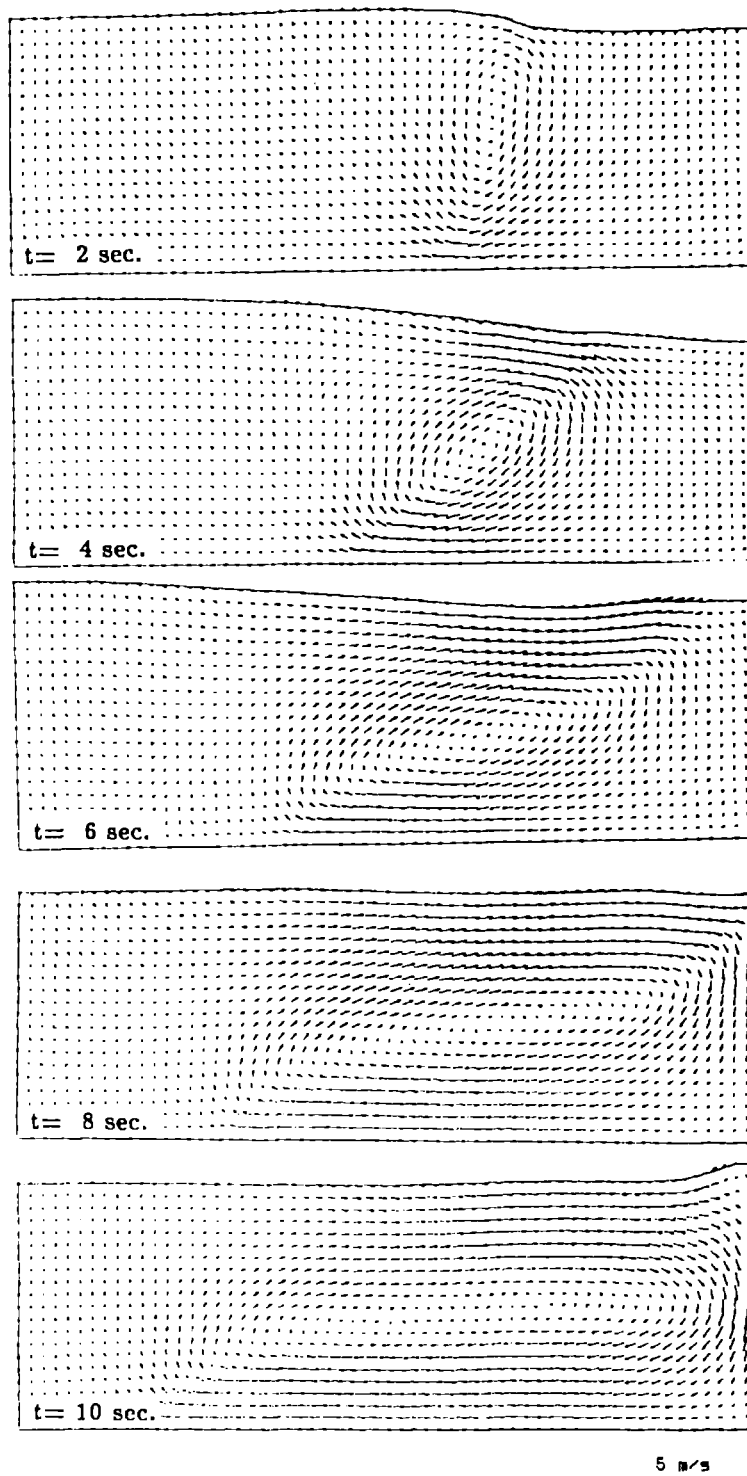


Figure 9. Velocity vector at times $t=2$, 4, 6, 8 and 10 s ($R_\rho=200$)

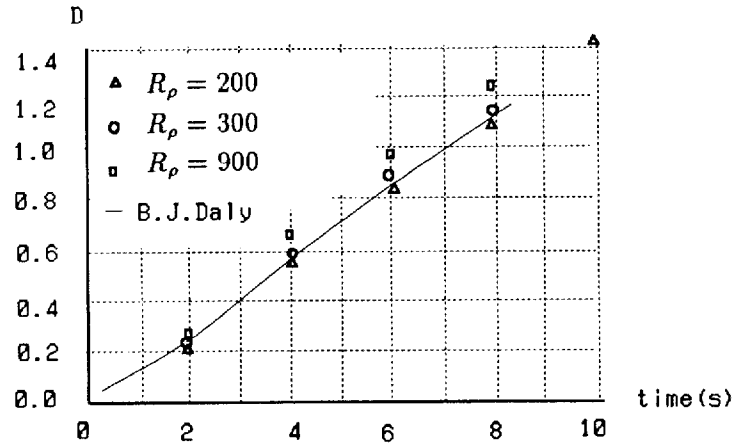


Figure 10. Density front position versus time

effect upon the subsequent motion of the fluids, the confined flow model[25] is not considered here and the movement of the free surface is described by

$$\frac{\partial \eta}{\partial t} + u_1 \eta_{,1} - u_2 = 0, \tag{36}$$

where $\eta$ is the elevation of the free surface. The pressure is zero on the free surface and the slip velocity boundary condition is applied on the solid boundary.

For $R_\rho = 200$ the distributions of markers at $t = 2$, 4, 6, 8 and 10 s are shown in Figure 8 and the velocity vectors are shown in Figure 9. At the initial stage, e.g. $t \leqslant 4$ s, the free surface of the right side decreases owing to the heavier fluid moving towards the left-down direction. At $t \geqslant 4$ s the free surface of the right side increases owing to the lighter fluid in the upper layer moving towards the right direction. This results in a large velocity recirculation region. The maximum recirculation velocity is about 5 m s$^{-1}$, which indicates that the flow is a convection-dominated one. The configurations of the two fluids can be identified clearly by the different markers. By defining the front position $D$ as $D = (L - L_0)/H$, where $L_0 = H$ is the distance occupied by the heavier fluid at time $t = 0$ and $L$ is the distance measured at the bottom of the container occupied by the same fluid, the front position versus time can be calculated as shown in Figure 10. The numerical results obtained by Daly and Parcht[25] are also plotted in the same figure. Their computations are stable under densimetric Froude number $R_\rho = 200$–$300$ and the numerical results are compared with the experimental observation. The present calculations are stable under $R_\rho = 200$–$900$ and the results obtained are in agreement with the literature.[25] The accuracy of the results is better than that of the lumping finite element method.[26,27] In the simulations of References 26 and 27 an artificial diffusion coefficient is introduced which is much larger than the physical viscosity of the fluid; thus the results do not change with the densimetric Froude number.

## 7. CONCLUSIONS

The three-step finite element method retains the third-order accuracy and uniform CFL property of the Taylor–Galerkin method. Since no new higher-order derivative term occurs in the numerical formulations, the present method is suitable for non-linear multidimensional convection-dominated flows and problems with complex boundary conditions. Owing to its extremely

simple algorithm, the present method can be applied to three-dimensional problems without any modification.

This method has been extended to solve unsteady incompressible flows. The numerical examples show that the present method is computationally efficient and the numerical results obtained are in good agreement with the literature.

ACKNOWLEDGEMENTS

The authors wish to thank the referees for their helpful comments. We would like to thank Dr. K. Kashiyama and Mr. K. Hatanaka for useful discussions. This research has been supported by the 1992 Chuo Grant for special research. The computations were carried out using the FACOM VP-30 computer of Chuo University

REFERENCES

1. A. N. Brooks and T. J. R. Hughes, 'Streamline upwind/Petrov–Galerkin formulation for convection dominated flows with particular emphasis on the incompressible Navier–Stokes equations', *Comput. Methods Appl. Mech. Eng.*, **32**, 199–259 (1982).
2. T. J. R. Hughes and A. N. Brooks, 'A multi-dimensional upwind scheme with no crosswind diffusion', in T. J. R. Hughes (ed.) *Finite Element Methods for Convection Dominated Flows*, AMD Vol. **34**, ASME, New York, 1979.
3. T. J. R. Hughes and T. E. Tezduyar, 'Finite element methods for first-order hyperbolic systems with particular emphasis on the compressible Euler equations', *Comput. Methods Appl. Mech. Eng.*, **45**, 217–284 (1984).
4. T. E. Tezduyar and T. J. R. Hughes, 'Development of time-accurate finite element techniques for first-order hyperbolic systems with particular emphasis on the compressible Euler equations', *Report Prepared underNASA–Ames University Consortium Interchange NCA2-0R745104*, 1982.
5. T. E. Tezduyar and T. J. R. Hughes, 'Finite element formulations for convection dominated flows with particular emphasis on the compressible Euler equations', *AIAA Paper 83-0125, Proc. AIAA 21st Aerospace Sciences Meeting*, Reno, NV, 1983.
6. T. E. Tezduyar and D. K. Ganjoo, 'Petrov–Galerkin formulations with weighting functions dependent upon spatial and temporal discretization: applications to transient convection–diffusion problems', *Comput. Methods Appl. Mech. Eng.*, **59**, 49–71 (1985).
7. J. Donea, 'A Taylor–Galerkin method for convective transport problems', *Int. j. numer. methods eng.*, **20**, 101–119 (1984).
8. J. Donea, S. Giuliani, H. Laval and L. Quartapelle, 'Time-accurate solution of advection–diffusion problems', *Comput. Methods Appl. Mech. Eng.*, **45**, 123–146 (1984).
9. J. Donea, L. Quartapelle and V. Selmin, 'An analysis of time discretization in the finite element solution of hyperbolic problems', *J. Comput. Phys.*, **70**, 463–499 (1987).
10. V. Selmin, J. Donea and L. Quartapelle, 'Finite element methods for nonlinear advection', *Comput. Methods Appl. Mech. Eng.*, **52**, 817–845 (1985).
11. M. Kawahara. 'Convergence of finite element Lax–Wendroff method for linear hyperbolic differential equation', *Proc. JSCE*, No 253, 95–107 (1976).
12. R. Lohner, K. Morgan and O. C. Zienkiewicz, 'The solution of non-linear hyperbolic equation systems by the finite element method', *Int. j. numer. methods fluids*, **4**, 1043–1063 (1984).
13. H. Laval and L. Quartapelle, 'A fractional-step Taylor–Galerkin method for unsteady incompressible flows', *Int. j. numer. methods fluids*, **11**, 501–513 (1990).
14. C. B. Jiang, M. Kawahara and K. Kashiyama, 'A Taylor–Gelerkin-based finite element method for turbulent flows', *Fluid Dyn. Res.*, **9**, 165–178 (1992).
15. P. M. Gresho, S. T. Chan, R. L. Lee and C. D. Upson, 'A modified finite element method for solving the time-dependent, incompressible Navier–Stokes equations, Part 1: Theory', *Int. j. numer. methods fluids*, **4**, 557–598 (1984).
16. D. M. Hawken, H. R. Tamaddon-Jahromi, P. Townsend and M. F. Webster, 'A Taylor–Galerkin-based algorithm for viscous incompressible flow', *Int. j. numer. methods fluids*, **10**, 327–351 (1990).
17. D. M. Hawken, P. Townsend and M. F. Webster, 'A finite element simulation of viscous flow around a cylinder', *Proc. Int. Conf. on Numerical Methods in Engineering: Theory and Applications*, Swansea, January 1990, pp. 955–962.
18. M. F. Webster and P. Townsend, 'Development of a transient approach to simulate Newtonian and non-Newtonian flow', *Proc. Int. Conf. on Numerical Methods in Engineering: Theory and Applications*, Swansea, January 1990, pp. 1003–1012.
19. P. M. Gresho and R. Sani, 'On pressure boundary conditions for the incompressible Navier–Stokes equations', *Int. j. numer. methods fluids*, **7**, 1111–1145 (1987).

20. M. Shimura and O. C. Zienkiewicz, 'Interaction analysis between structure and fluid flow using the direct Laplacian method', *Proc. 4th Int. Conf. on Computing in Civil and Building Engineering*, Tokyo, July 1991, pp. 267–274.
21. M. Nallasamy and K. Krishna Prasad, 'On cavity flow at high Reynolds number', *J. Fluid Mech.*, **79**, 391–414 (1977).
22. S. Sivaloganathan and G. J. Shaw, 'A multigrid method for recirculating flows', *Int. j. numer. methods fluids*, **8**, 417–440 (1988).
23. U. Ghia, K. N. Ghia and C. T. Shin, 'High-*Re* solutions for incompressible flow using the Navier–Stokes equations and a multigrid method', *J. Comput. Phys.*, **48**, 387–411 (1982).
24. R. Schreiber and B. Keller, 'Driven cavity flows by efficient numerical techniques', *J. Comput. Phys.*, **49**, 310–333 (1983).
25. B. J. Daly and W. E. Parcht, 'Numerical study of density-current surges', *Phys. Fluids*, **11**, 15–30 (1968).
26. B. Ramaswamy, 'Numerical simulation of unsteady viscous free surface flow', *J. Comput. Phys.*, **90**, 396–430 (1990).
27. M. Kawahara and K. O. Ohmiya, 'Finite element analysis of density flow using the velocity correction method', *Int. j. numer. methods fluids*, **5**, 981–993 (1987).